WATER RESOURCES RESEARCH, VOL. 37, NO. 6, PAGES 1783–1793, JUNE 2001

Effect of sorbed oil on the dielectric properties of sand and clay

Camille Li,[1] Paulette Tercier, and Rosemary Knight[2]

Department of Earth and Ocean Sciences, University of British Columbia, Vancouver, British Columbia, Canada

Abstract. The dielectric response of geologic materials is related to the amount of water-wetted solid surface present. This dependence raises the possibility that dielectric measurements may be used to detect changes in the state of the solid-fluid interface such as those caused by the sorption of a chemical species. In this study, complex impedance data are collected for systems of clean and oil-bearing sand and kaolinite vacuum-saturated with a 0.001 *M* NaCl brine in the frequency range 100 kHz to 10 MHz. The effective dielectric constant κ and electrical conductivity σ of the samples are calculated from these measurements assuming quasi-static conditions. We define the components in our system as brine, air, and a "wetted" solid phase. In this way, the contribution of the solid-fluid interface to the bulk dielectric response is included in the last component. We use an inclusion-based effective medium theory to extract the dielectric response of the wetted solid from the experimental data. The presence of sorbed oil is found to have little effect on the dielectric response of the wetted sand matrix, presumably because of the very low surface area (0.2 m^2/g) of the solid-fluid interface. In contrast, the kaolinite (5–12 m^2/g) data indicate a decrease of the order of 50% in the dielectric constant of the wetted matrix phase as the amount of water-wetted surface in the sample decreases. The results from this experimental study show that the presence of sorbed oil leads to a detectable change in the dielectric properties of high surface area geologic materials.

1. Introduction

Measurement of the dielectric response of geologic materials can provide useful information about in situ properties. For example, it is well known that dielectric properties are affected by the presence of water, and measurement of the dielectric response of soils with time domain reflectometry is commonly used as a means of determining water content.

In addition to this sensitivity to water content, it has also been shown that the size of the water-wetted solid surface has a significant effect on the dielectric response of geologic materials [*Lange*, 1983; *Knight and Nur*, 1987]. The wetting of the solid surface by a few monolayers of water has been shown to increase the measured dielectric constant to a much larger extent than would be predicted by solely accounting for the volume of water added and is due to contributions to the bulk dielectric response from the properties of the solid-water interface [*Knight and Endres*, 1990]. These observations raise the possibility that dielectric measurements can be used to detect variations at the solid-water interface, such as a change in wettability of the solid or the sorption of chemical species. Such an idea is supported by previous studies which have shown that the dielectric response changes significantly when the surface properties of sandstones are altered by various chemical treatments [*Knight and Abad*, 1995], with the differences becoming more apparent at frequencies below 10 kHz [*Börner et al*., 1993; *Garrouch and Sharma*, 1990]. The specific interest of the present study is to assess the use of dielectric measurements to detect the presence of oil sorbed to the solid surface. If the effect of sorbed oil on the dielectric response can be isolated and quantified, it might be possible to use dielectric measurements, in the laboratory or in the field, as a noninvasive means of detecting residual amounts of such contaminants.

If we consider the bulk or total dielectric permittivity of a multicomponent material to be due to the volume fractions and permittivities of the individual components, then the contribution from the solid-fluid interface can be accounted for by allowing our definition of the solid phase to incorporate the properties of this interface. That is, rather than treating our rock-fluid system as being composed of a dry solid phase and the contained fluid phases, we define our rock-fluid system as being composed of the "wetted" solid phase and the contained fluid phases. We allow the dielectric contribution from the solid-fluid interface to be part of the dielectric properties of the solid. This was the approach taken by *Knight and Endres* [1990]. While this method lacks any fundamental treatment of the mechanisms responsible for the dielectric response of the solid-fluid interface, it serves the purpose of isolating the role of the interface from the contributions of the bulk fluid and solid phases to the bulk dielectric response. The key idea is that if we can extract the dielectric response of the wetted matrix from our measurement of the bulk dielectric response of the fluid-saturated material, we can obtain information about the state of the solid-fluid interface. This approach will thus allow us to determine the way in which the dielectric response of the wetted matrix changes with the sorption of increasing amounts of oil.

In this study, we determine the dielectric behavior of geo-

[1]Now at Department of Atmospheric Sciences, University of Washington, Seattle, Washington.

[2]Now at Department of Geophysics, Stanford University, Stanford, California.

Paper number 2001WR900006.
0043-1397/01/2001WR900006$09.00

logic materials in a "clean" water-wet state and with various amounts of sorbed oil. We used both a silica sand and kaolinite, the higher surface area of the clay allowing us to better observe the behavior of the solid-fluid interface. An inclusion-based effective medium theory (IBEMT) is used to isolate the dielectric response of the wetted solid phase in order to assess the effect of oil sorption on this parameter. Results from this study will allow us to better understand the role of the solid-fluid interface in determining dielectric behavior and contribute to the development of methodologies for using dielectric measurements to detect small amounts of sorbed organic contaminants in both laboratory and field applications.

2. Definition of Terms

Over time, inconsistencies in the definition of constitutive relationships, parameters, and sign conventions have developed as different investigators tailor the governing equations of electromagnetic theory to their work. For clarity, we will define the terms and notation used here.

In general, the electrical conductivity $\sigma^*(\omega)$ and permittivity $\varepsilon^*(\omega)$ are complex, frequency-dependent parameters which describe the microscopic electromagnetic properties of a material. Following the sign convention adopted by *Ward and Hohmann* [1988], these parameters will be defined as

$$\sigma^*(\omega) = \sigma'(\omega) + i\sigma''(\omega), \tag{1}$$

$$\varepsilon^*(\omega) = \varepsilon'(\omega) - i\varepsilon''(\omega). \tag{2}$$

In the laboratory, we measure the complex impedance of samples. As shown in section 3.3, two "effective" parameters can be extracted from the complex impedance measurement. The effective permittivity $\varepsilon_{ef}(\omega)$ represents the ability of the material to store charge through polarization and is given by

$$\varepsilon_{ef}(\omega) = \varepsilon'(\omega) + \frac{\sigma''(\omega)}{\omega}, \tag{3}$$

where $\varepsilon'(\omega)$ is the polarization term and $\sigma''(\omega)$ is a Faradaic diffusion loss term. Both of these terms describe mechanisms associated with charge polarization; however, as it is impossible to distinguish between the contribution from each in a complex impedance measurement, they remain combined in the parameter defined as $\varepsilon_{ef}(\omega)$.

Similarly, the effective conductivity $\sigma_{ef}(\omega)$ represents the ability of the material to transport charge and is given by

$$\sigma_{ef}(\omega) = \sigma'(\omega) + \omega\varepsilon''(\omega), \tag{4}$$

where $\sigma'(\omega)$ is the ohmic conduction and $\varepsilon''(\omega)$ is a loss due to polarization lag. Again, we note that although charge transport within the material is a result of two very different mechanisms, we measure only the combined effect in the parameter defined as $\sigma_{ef}(\omega)$.

In developing models to describe the dielectric behavior of multicomponent materials it is convenient to incorporate the two effective parameters into one, the total complex permittivity $\varepsilon^*_T(\omega)$, defined as

$$\varepsilon^*_T(\omega) = \varepsilon_{ef}(\omega) - (i/\omega)\sigma_{ef}(\omega). \tag{5}$$

Using (3) and (4), the expression for the total complex permittivity can be expanded and the terms rearranged to yield

$$\varepsilon^*_T(\omega) = [\varepsilon'(\omega) - i\varepsilon''(\omega)] - (i/\omega)[\sigma'(\omega) + i\sigma''(\omega)]. \tag{6}$$

It is commonly assumed in modeling studies that $\sigma''(\omega) = 0$ and that $\sigma'(\omega) = \sigma_{DC}$, the frequency-independent DC conductivity of the material [*Sen et al*., 1981; *Feng and Sen*, 1985; *Endres and Knight*, 1992]. All frequency dependence in the effective parameters is attributed to the real and imaginary parts of the complex permittivity, including a contribution from the relaxation of bound charges at higher frequencies through the $\omega\varepsilon''(\omega)$ term.

For notational simplicity, the (ω) designation will be dropped for the remainder of the discussion. We will use σ to represent the effective conductivity and κ, defined as

$$\kappa = \varepsilon_{ef}/\varepsilon_0, \tag{7}$$

to represent the quantity commonly referred to as the "dielectric constant," which is, in fact, the effective dielectric permittivity normalized to the permittivity of free space ($\varepsilon_0 = 8.85 \times 10^{-12}$ F/m).

3. Experimental Procedure

3.1. Sample Description and Preparation

The silica sand used in this study was obtained from Wedron Silica Sand Company. It contains 99.88% silicon dioxide (SiO_2) with grain sizes between 120 and 140 U.S. standard mesh (105–125 μm). The kaolinite is a well-crystallized clay with structural formula $Al_4[Si_4O_{10}](OH)_8$ obtained from the Source Clay Mineral Repository at the University of Missouri, Columbia. The median particle size is 0.7 μm, with over 90% (by mass) of the grains <2 μm in diameter [*Zbik and Smart*, 1998]. Laboratory measurements were made on these materials both in their natural hydrophilic or water-wet state ("clean") and with various amounts of sorbed oil. The clean sand sample, referred to as S, was washed with an HCl solution and rinsed repeatedly with distilled, deionized water, while the kaolinite in its natural state, referred to as K, was considered clean.

Three of the clay samples with sorbed oil (KO5, KO22, and KO70) were prepared by a sorption method involving a week of tumbling with a solution of crude oil (Cold Lake bitumen provided by Imperial Oil) dissolved in *n*-heptane and toluene. Varying the initial oil concentration in the solutions made it possible to vary the amount of sorbed oil. While previous studies have found that the surface properties of clays can be affected by organic solvents, such as toluene or heptane [*Santamarina and Fam*, 1997; *Vanhala et al*., 1992; *Olhoeft*, 1992], it is important to note that these solvents were used in our study only as a way to introduce crude oil into the pore space. Higher molecular weight organic molecules will outcompete lower molecular weight molecules for the surface sites [*Stumm*, 1992], such that crude oil will be preferentially sorbed to the kaolinite. The amount of oil sorbed to a clay sample was determined by measuring the amount of oil lost from the bitumen solution and is given as the numbers (5, 22, and 70) at the end of the sample name with units of milligrams per gram of clay. The amount of oil in the bitumen solution was measured using a UV/Visible 4050 spectrophotometer ultraspec II (λ = 402 nm) calibrated to a set of standard solutions with known oil concentrations.

The fourth clay, KO, and the sand sample referred to as SO were first rendered hydrophobic by treatment with a chemical called octadecyltrichlorosilane purchased from Sigma of the Sigma-Aldrich Corporation, then exposed to a concentrated version of the above bitumen solution for 10 min. The samples

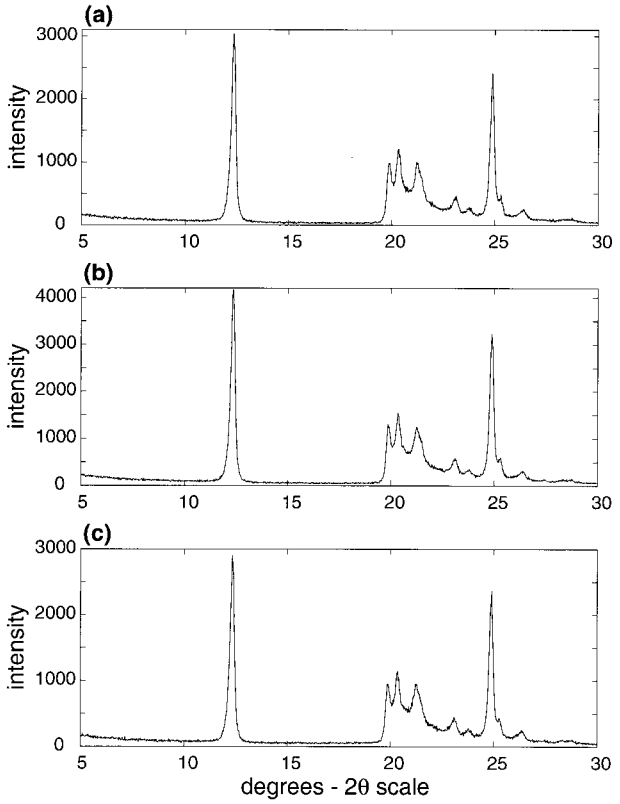

Figure 1. X-ray diffraction patterns for the (a) clean (K), (b) hydrophobic, and (c) oil-bearing hydrophobic (KO) kaolinite samples collected on a Siemens D5000 powder X-ray diffractometer with $\lambda = 1.5406 \times 10^{-10}$ m.

were vacuum-filtered from the bitumen solutions and left in a fumehood for several days to allow any remaining toluene and heptane to volatilize.

A Siemens D5000 powder X-ray diffractometer was used to examine the crystal structure of the kaolinite samples both before and after surface treatments. The identical X-ray diffraction patterns collected for the clean, hydrophobic, and oil-bearing hydrophobic clays (see Figures 1a–1c, respectively) imply that neither the silanization procedure nor the oil sorption alters the crystal structure of the solid kaolinite matrix. Grain density values were measured using a Micromeritics helium pycnometer and appear in Table 1. Note that owing to the additional surface treatment and hence extra silane layer, on sample KO, it displays a significantly lower grain density than the other samples.

Table 1. Sample Descriptions: Parameters for the Two Silica Sand and Five Kaolinite Samples Used in the Study

Sample	Grain Density,[a] g/cm^3 (±0.08)	Porosity ϕ[a] (±0.03)	S_w (±0.03)	Adsorbed Oil, mg oil/g clay
S	2.71	0.54	0.94	
SO	2.71	0.46	0.90	
K	2.62	0.50	0.94	
KO	2.36	0.50	0.96	30
KO5	2.61	0.50	0.94	5
KO22	2.58	0.48	1.00	22
KO70	2.53	0.50	0.97	70

[a]Micromeritics He pycnometer measurements (University of British Columbia's Rock Physics Laboratory, Vancouver).

One obvious approach to characterizing the clay surfaces in the various samples is by the amount of sorbed oil present. Given the methods of sample preparation, we initially expected this property to range from zero on sample K to a maximum value on sample KO. However, using the grain density measurements and the known densities of silane and crude oil, we found sample KO to bear ~30 mg of oil per gram of clay, less than the amount on sample KO70. The pretreatment with the silane apparently did not increase the tendency of the sample to sorb oil.

As earlier studies had suggested the role of the water-wetted surface area in determining κ, we used a water sorption experiment to characterize the relative amount of water-wetted surface on each of the clay samples. The samples were compressed into consolidated discs with porosities of 50%. The discs were placed in a Blue M controlled temperature/humidity chamber. With the temperature fixed at 25°C, the humidity inside the chamber was incrementally increased from 40 to 90%, and the mass of the samples at each step was measured. The amount of water sorbed was calculated by subtracting the dry weight of the clays measured after a 1 week storage period over a $CaSO_4$ dessicant. The mass of sorbed water is a reflection of the sample's affinity for water and therefore provides a relative measure of the size of the water-wetted surface area.

3.2. Determining Pore Fluid Conductivity

When an aqueous solution comes into contact with a solid surface, its conductivity can be altered as a result of chemical reactions between the solid and the fluid. The extent of the conductivity change depends on factors, such as temperature, time, the chemical nature of the rock, the surface area of the rock-fluid interface, and the salinity and pH of the solution. Because these experiments involve numerous different surface types, each with their own associated chemical species, we expect the pore fluid in each sample to be affected differently. The resulting variations in conductivity must be accounted for in the analysis of the dielectric measurements.

In selecting a suitable saturating fluid for the experiments we attempted to satisfy the requirements that the fluid be representative of natural groundwater and that its salinity be sufficiently high to swamp small temporal changes in fluid conductivity due to solid-fluid chemical reactions. In order to determine the magnitude of changes in fluid conductivity caused by contact with our solid samples, four glass vials were prepared, each containing ~2.5 g of sand or clay (S, SO, K, or KO) and 25 mL of distilled water. The vials were tumbled in an environmental chamber regulated at 20°C, and the electrical conductivity of the pore fluid σ_b was monitored over a period of 6 weeks. From these σ_b measurements we determined that a 0.001 *M* NaCl brine (0.011 S/m at 20°C) would be capable of swamping variations in the conductivity of the pore fluids due to the different surface types. Unfortunately, when the last three oil-bearing kaolinite samples were prepared, we found that this was not the case with KO70. Owing to the large amount of sorbed oil in KO70 the soluble impurities from the oil are able to cause pore fluid conductivity changes from the initial value, even when relatively saline solutions are used. To ensure that we had reliable values of pore fluid conductivity for our analysis, we designed a method to estimate this parameter for all the samples.

Glass vials were filled with ~5 g of each sample and 25 mL

Table 2. Pore Fluid Conductivity

Sample	σ'_b, S/m
S	0.010 ± 0.001
SO	0.010 ± 0.001
K	0.012 ± 0.003
KO	0.013 ± 0.003
KO5	0.013 ± 0.003
KO22	0.013 ± 0.003
KO70	0.074 ± 0.008

of the 0.001 *M* NaCl solution and set to tumble in an environmental chamber regulated at 20°C. At periodic intervals (every day during the first week, then every 2 days) the electrical conductivity of the solutions was measured with a probe. After ~9 weeks, the values had stabilized, and these were taken to be the pore fluid conductivities for the samples (shown in Table 2). Three vials were prepared for each sample type, and the discrepancy between measurements was used to estimate the uncertainty of the σ_b values. As expected, there was no significant difference in pore fluid conductivities from the initial σ_b of 0.011 S/m for the silica sand and kaolinite samples except for KO70, where the presumed leeching of large amounts of soluble impurities increased σ_b to a value of 0.0745 S/m.

3.3. Electrical Measurements

For the electrical measurements, the samples were contained in a two-electrode parallel-plate sample holder consisting of two gold-sputtered copper electrodes, each 4.225 ± 0.003 cm in diameter, which fit into a Plexiglass ring that fixes the sample thickness at 0.448 ± 0.003 cm. A Hewlett Packard 4192a low-frequency impedance analyzer was used to measure the complex admittance Y^* of the samples

$$Y^* = G_p + i\omega C_p, \tag{8}$$

where G_p is the parallel conductance, C_p is the parallel capacitance, and ω is the angular frequency. The effective conductivity σ and dielectric constant κ were computed from these measured parameters assuming quasi-static conditions, in which magnetic effects and higher-order terms of the electric field are ignored [*Shen et al*., 1985] to arrive at the solutions

$$\sigma = (G_p d)/A,$$
$$\kappa = (C_p d)/A\varepsilon_0, \tag{9}$$

where A is the cross-sectional area of the sample and d is its length. Tests with Stycast HiK dielectric standards have shown this experimental setup capable of determining σ and κ to within a range of ±2% [*Li*, 1999].

The complex admittance of the two sand samples and five kaolinite samples under room-dry and brine-saturated conditions was measured at a series of frequencies spaced logarithmically between 500 Hz and 10 MHz, with the peak-to-peak oscillation amplitude of the input signal set at 1 volt. Once packed into the holder, the unsaturated or room-dry sample was placed in a vacuum chamber and evacuated to 15 μm of mercury. A 0.001 *M* NaCl solution was introduced into the chamber, and an intensifier was used to increase the pressure in the system to 1400 kPa. The sample was left in the pressurized chamber overnight, and the difference in its mass before and after saturation was used to calculate the water content, S_w, which is defined as the volume fraction of the pore space filled with water. The physical properties of each sand and clay sample appear in Table 1.

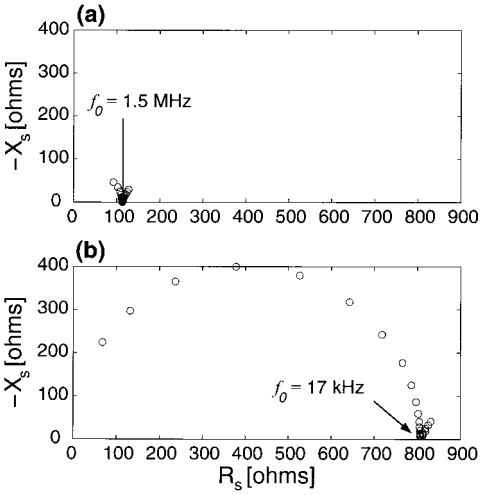

Figure 2. Complex impedance plots for clean silica sand (S) samples saturated with (a) a 0.01 *M* NaCl brine and (b) a 0.001 *M* NaCl brine over the frequency range 500 Hz to 10 MHz.

Following the method described by *Knight and Nur* [1987], the data were plotted in the complex impedance plane in order to isolate the portion of the data set containing the desired bulk sample response from the portion which is corrupted by electrode effects. A complex impedance plot, such as those in Figure 2, represents the electrical response of a sample in terms of the reactance X_s and series resistance R_s, given by the relationships

$$R_s = \frac{1/G_p}{1 + (\omega C_p/G_p)^2},$$
$$X_s = -\frac{\omega C_p/G_p^2}{1 + (\omega C_p/G_p)^2}. \tag{10}$$

Frequency increases down the tail segment and counterclockwise around the semicircular portion of the plot. Studies have identified the low-frequency tail as a response from the sample-electrode interface, while the high-frequency semicircle represents the bulk sample response which we are interested in [*Raistrick et al*., 1976]. For less ideal (i.e., more lossy) materials such as clays, the semicircle becomes depressed, and the angle of the tail from the vertical increases.

Figure 2a shows data collected from a sample saturated with a 0.01 *M* NaCl brine. A significant number of data points here have been corrupted by electrode effects and hence lie in the tail segment of the complex impedance plot. In fact, only data above the cutoff frequency f_0 of 1.5 MHz represent the true sample response. On the other hand, the sample saturated with a 0.001 *M* brine (Figure 2b) yielded more data along the semicircle (f_0 = 17 kHz), meaning that a larger proportion of this data set could be used. Complex impedance plots such as these were constructed for each data set collected in order to determine the useful frequency range for the various samples.

4. Model Development

A theoretical model representing the electrical properties of a heterogeneous system aims to construct an expression for the

bulk response given a description of its various components. Among the diverse approaches to constructing a mathematical formulation that accurately represents the response of real geologic materials are phenomenological models [*Debye*, 1929; *Cole and Cole*, 1941], effective medium theories [*Jackson*, 1975; *Sen et al*., 1981], and volumetric mixing laws, such as the complex refractive index method (CRIM) [*Wharton et al*., 1980]. CRIM predicts the bulk permittivity ε^*_T of a material given only the permittivities ε^*_i and volume fractions f_i of each of the i components:

$$\sqrt{\varepsilon^*_T} = \sum_i f_i \sqrt{\varepsilon^*_{T,i}}. \tag{11}$$

Inclusion-based effective medium theories constitute another genre of mathematical model and are commonly used to investigate the behavior of multiphase media. Fundamental to this type of model is the concept that a heterogeneous material can be depicted in terms of a background component into which incrementally small inclusions of other components are embedded. In the case of our brine-saturated sand and kaolinite systems, we define the three components to be air, brine, and a "wetted matrix" which combines any surface layer of water at the solid-fluid interface with the rock grains to form the solid phase. This approach allows for surface effects, including additional polarization mechanisms arising from electrochemical phenomena and nonspherical grains, to be incorporated into the wetted matrix parameter. The IBEMT used to describe the material is a form of *Feng and Sen*'s [1985] differential formula,

$$\frac{d\varepsilon^*_T}{3\varepsilon^*_T} = \frac{dv_{wm}}{v_T}\frac{\varepsilon^*_{T,wm} - \varepsilon^*_T}{\varepsilon^*_{T,wm} + 2\varepsilon^*_T} + \frac{dv_a}{v_T}\frac{\varepsilon^*_{T,a} - \varepsilon^*_T}{\varepsilon^*_{T,a} + 2\varepsilon^*_T}, \tag{12}$$

where the subscripts wm and a refer to the wetted matrix and air and v_T is the total volume. For a material with porosity ϕ and water saturation S_w we make the assumption that

$$\frac{dv_a}{dv_{wm}} = \frac{(1 - S_w)\phi}{1 - \phi} \equiv \eta. \tag{13}$$

Fixing the ratio of volume increments allows us to rewrite the IBEMT as

$$\frac{d\varepsilon^*_T}{dv} = 3\varepsilon^*_T\left(\frac{\varepsilon^*_{T,wm} - \varepsilon^*_T}{\varepsilon^*_{T,wm} + 2\varepsilon^*_T} + \eta\frac{\varepsilon^*_{T,a} - \varepsilon^*_T}{\varepsilon^*_{T,a} + 2\varepsilon^*_T}\right), \tag{14}$$

where $v = v_{wm}$. An implicit solution is presented by *Feng and Sen* [1985] and gives the dielectric response through the expression

$$S_w\phi = \left(\frac{\varepsilon^*_{T,b}}{\varepsilon^*_T}\right)^{1/3}\left(\frac{a(\varepsilon^*_T)^2 + b\varepsilon^*_T + c}{a(\varepsilon^*_{T,b})^2 + b\varepsilon^*_{T,b} + c}\right)^{1/2}$$
$$\cdot\left(\frac{(2a\varepsilon^*_T + b - \sqrt{b^2 - 4ac})(2a\varepsilon^*_{T,b} + b + \sqrt{b^2 - 4ac})}{(2a\varepsilon^*_T + b + \sqrt{b^2 - 4ac})(2a\varepsilon^*_{T,b} + b - \sqrt{b^2 - 4ac})}\right)^m, \tag{15}$$

where

$$a = -2(1 + \eta), \tag{16}$$

$$b = 2\varepsilon^*_{T,wm} - \varepsilon^*_{T,a} + \eta(2\varepsilon^*_{T,a} - \varepsilon^*_{T,wm}), \tag{17}$$

$$c = \varepsilon^*_{T,wm}\varepsilon^*_{T,a}(1 + \eta), \tag{18}$$

$$\eta = \phi(1 - S_w)/(1 - \phi), \tag{19}$$

$$m = -\frac{(2\varepsilon^*_{T,wm} + \varepsilon^*_{T,a}) + \eta(2\varepsilon^*_{T,a} + \varepsilon^*_{T,wm})}{2\sqrt{b^2 - 4ac}}. \tag{20}$$

We used an alternate method involving the solution of (14) as an initial value problem. Since the inclusions are assumed to be randomly dispersed throughout the background brine, the new additions of wetted matrix and air at each step will not only replace brine but also a part of the previously introduced inclusions. This consideration sets the upper bound for v, and (14) can then be solved by numerically integrating with a fourth-order Runge-Kutta routine over

$$v = 0 \rightarrow \frac{1}{1 + \eta}\ln[\phi(1 + \eta) - \eta]^{-1}, \tag{21}$$

with the initial condition $\varepsilon^*_T(0) = \varepsilon^*_{T,b}$, the permittivity of the brine, at $v = 0$. In all cases, air was assigned a total permittivity of $\varepsilon^*_{T,a} = \varepsilon_0$, and the permittivity of the brine was set at $\varepsilon'_b = 80\varepsilon_0$ [*Feng and Sen*, 1985]. The porosity and saturation values were taken from Table 1, and the brine conductivities were taken from Table 2.

The algorithm used to recover the wetted matrix parameters given a data set of measured (or effective) bulk conductivities and dielectric constants is illustrated here with a simple example. In the case of real data, uncertainties in our measurement of σ_b, κ, σ, S_w, and ϕ are significant in determining the accuracy to which we can calculate the wetted matrix parameters. A series of tests on synthetic data sets incorporating error from these quantities allowed us to estimate the range of uncertainty for the results.

Consider a sample composed of rock, brine, and air on which a measurement at 1 MHz yields bulk properties of $\kappa = 15$ and $\sigma = 0.01$ S/m. In this example, we assume a brine conductivity of 0.02 S/m, $\phi = 0.35$, and $S_w = 0.95$. All other properties of the air and brine phases are assigned as described above.

The CRIM formula shown in (11) is used to estimate reasonable ranges within which the wetted matrix dielectric constant and conductivity are expected to lie. For m evenly spaced values of σ_{wm} and n evenly spaced values of κ_{wm} in these ranges the complex bulk electrical response ε^*_T is evaluated by solving (14). This step produces an $m \times n$ matrix of computed bulk permittivities, with each $\varepsilon^*_{T(m,n)}$ corresponding to a position on a grid of possible σ_{wm}, κ_{wm} pairs. In other words, if we place the σ_{wm}, κ_{wm} grid on the x, y plane of a three-dimensional plot, the conductivities and dielectric constants calculated from $\varepsilon^*_{T(m,n)}$ can be plotted on the z axis to form two surfaces, as shown in Figures 3a and 3b. Each surface intersects the measured data, represented by the meshes, along a curve. The wetted matrix parameters are given by the σ_{wm}, κ_{wm} pair at the position on the x, y plane where these curves intersect (see Figure 3c), which for this example, yields a solution of approximately $\sigma_{wm} = 0.01$ S/m and $\kappa_{wm} = 15$.

5. Results and Discussion

Complex impedance plots for the two sand samples and five kaolinite samples are shown in Figures 4 and 5, with the selected cutoff frequencies labeled on each plot. Note that clays display a more complicated complex plane response than sands due to an additional polarization mechanism. However, it is difficult to separate this clay polarization effect from the electrode effect, and we have therefore selected the clay cutoffs at the inflection in the high-frequency arc to ensure that the data

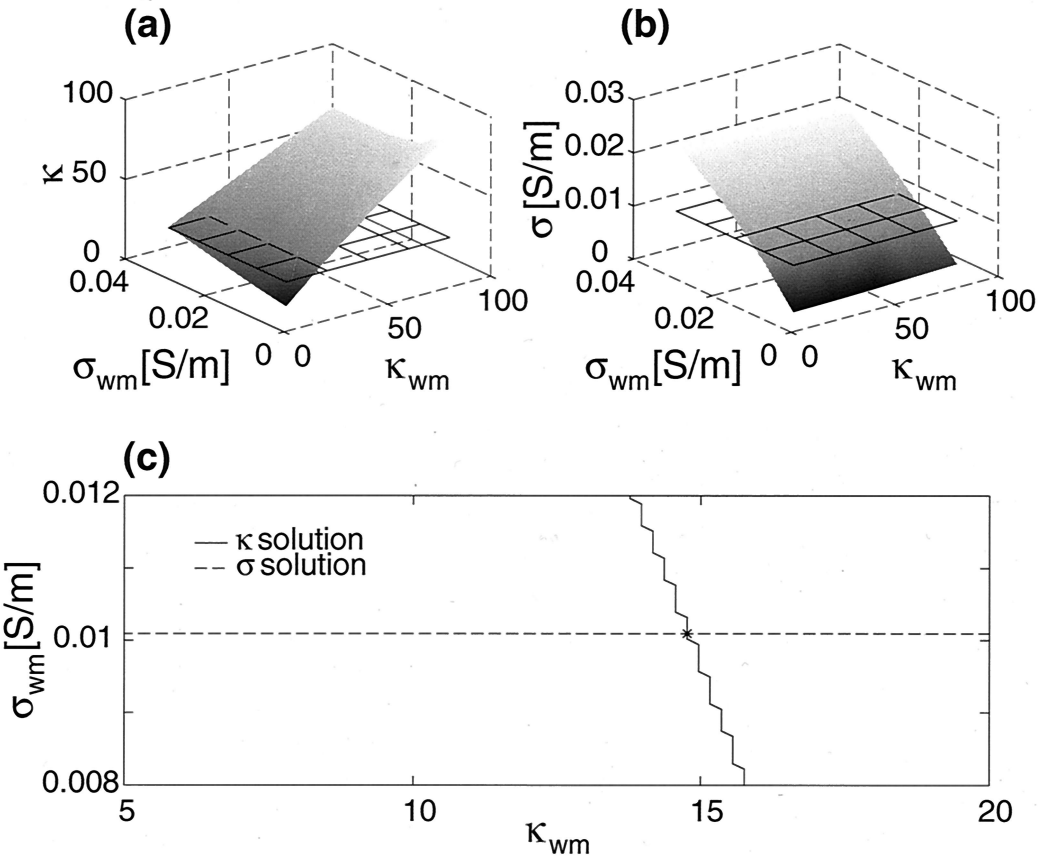

Figure 3. Example illustrating the method used to solve for wetted matrix parameters. (a) Effective dielectric constant κ and (b) conductivity σ surfaces are calculated for possible wetted matrix σ_{wm}, κ_{wm} pairs. (c) The curves where these surfaces match the measured κ and σ values intersect at the point on the σ_{wm}, κ_{wm} grid which yields the solution.

used contain only the bulk sample response. In our analysis, we will use all sand data above 100 kHz, data for kaolinite samples K, KO, KO5, and KO22 above 300 kHz, and data for kaolinite sample KO70 above 1 MHz. Calculated wetted matrix dielectric constants are accurate to within ±10% for sample KO70, ±17% for samples KO, KO5, and KO22, and ±19% for sample K, with the uncertainty largely due to the uncertainty in our measurement of brine conductivity.

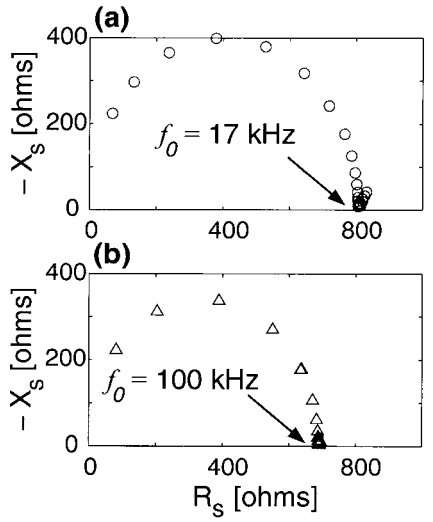

Figure 4. Complex impedance plots for silica sand samples (a) S (clean) and (b) SO (oil-bearing hydrophobic) over the frequency range 500 Hz to 10 MHz.

The bulk and wetted matrix responses over the frequency ranges of interest appear in Figures 6 and 7 for the sand samples and Figures 8 and 9 for the kaolinite samples. We have shown both κ and σ for each sample as both bulk parameters are required for the inversion, and both wetted matrix parameters are recovered; however, as we are mainly interested in the behavior of the dielectric constant, we will focus on these results.

The bulk dielectric constants of the clean silica sand sample and the sample with sorbed oil show little contrast in this frequency range (see Figure 6a), as was expected considering results from prior studies [*Börner et al.*, 1993; *Garrouch and Sharma*, 1990]. The wetted matrix dielectric constants were computed using the parameters given in Table 1 and Table 2 but again yielded very similar values (see Figure 7a). The wetted matrix dielectric constant is consistently greater at all frequencies for the water-wetted sand, a result that is in agreement with previous studies, but the difference is not large. Since the samples were identical apart from the nature of the grain surfaces, it is likely that the specific surface area of the sand is so low that changes in the interfacial response due to the presence of sorbed oil did not result in significant differences in the dielectric response.

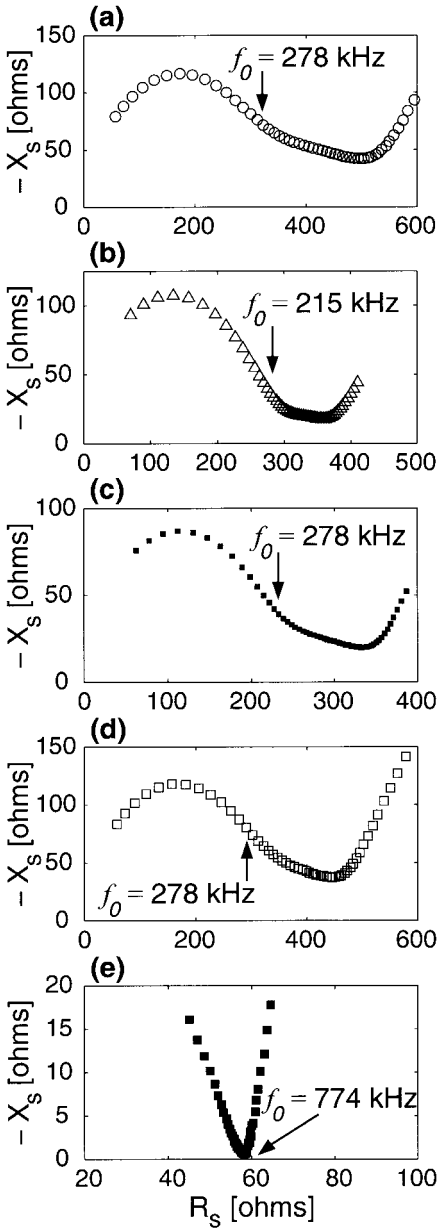

Figure 5. Complex impedance plots for kaolinite samples (a) K (clean), (b) KO (oil-bearing hydrophobic), (c) KO5 (5 mg/g oil-bearing), (d) KO22 (22 mg/g oil-bearing), and (e) KO70 (70 mg/g oil-bearing) over the frequency range 500 Hz to 10 MHz.

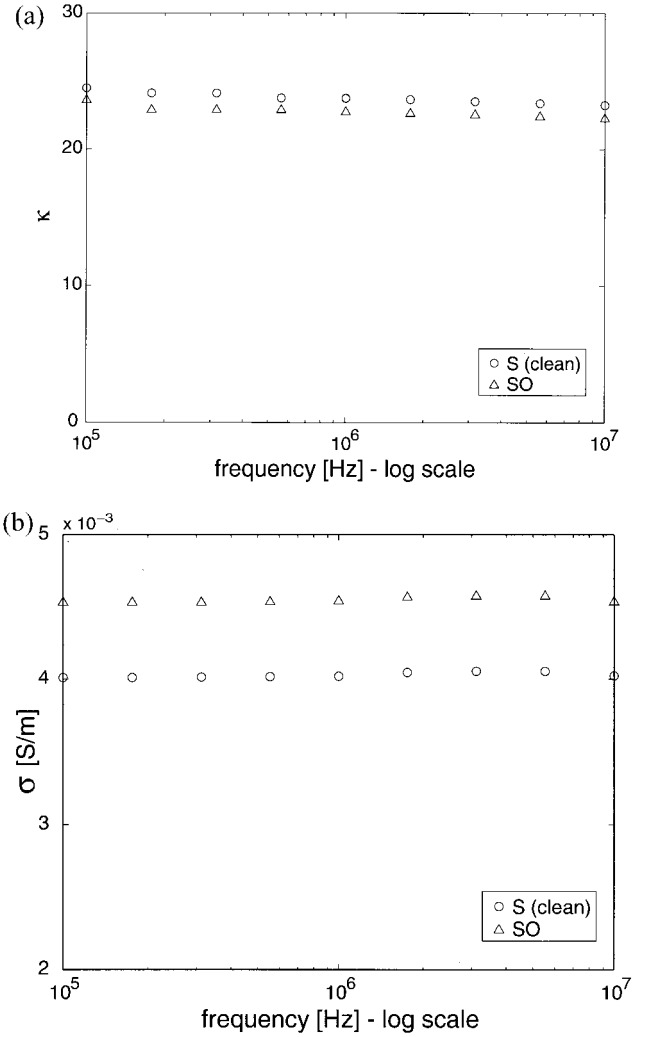

Figure 6. (a) Bulk dielectric constant κ and (b) bulk conductivity σ for sand samples (1) S (clean) and (2) SO (oil-bearing hydrophobic) over the frequency range 100 kHz to 10 MHz.

The kaolinite samples produced unmistakably distinct responses as seen in Figure 8a, where we show the bulk dielectric constant as a function of frequency. The solid lines on the plot represent the measured response of the unsaturated samples. Again, we computed the wetted matrix dielectric constants using the appropriate parameters for each sample, and these are shown in Figure 9a. In order to facilitate comparison of the kaolinite data sets, Figure 9a is limited to frequencies above 1 MHz, the selected cutoff for sample KO70. Note here that there are several crossovers in the κ_{wm} responses for various samples. Whereas the bulk dielectric constant of KO is less than that of KO70 over the entire frequency range, the wetted matrix dielectric constant of KO70 dips at ~6 MHz. Samples KO5 and KO22, whose bulk dielectric constants converge above 1 MHz, also exhibit intersecting κ_{wm} responses. One possible reason is that the quasi-static assumption is only valid while $|ka| \ll 1$ [*Shen et al.*, 1985], where a is the sample radius and the wave number k is given by

$$k = (\omega^2\mu\varepsilon - i\omega\mu\sigma)^{1/2}. \tag{22}$$

For rocks we generally set $\mu = \mu_0$, the magnetic permeability of free space ($\mu_0 = 1.26 \times 10^{-6}$ N/A^2), and we find that for frequencies of the order of 10–100 MHz, $|ka|$ approaches unity. In other words, there are likely small, higher-order dynamic effects which are influencing our measurements but which we are not considering in our analysis.

Figure 10 shows the results of the water sorption experiment. This plot allows us to draw some conclusions about the amount of water-wetted surface area in each of the samples. The clean kaolinite sample (K) sorbed the most water and, consequently, can be said to have the largest water-wetted surface area. We see that for samples K, KO5, KO22, and KO70, as more oil is present on the sample, the amount of sorbed water decreases, an indication that the hydrophobicity has increased. Sample KO sorbs the least water, undoubtedly due to the presence of the silane layer that acts with the oil in

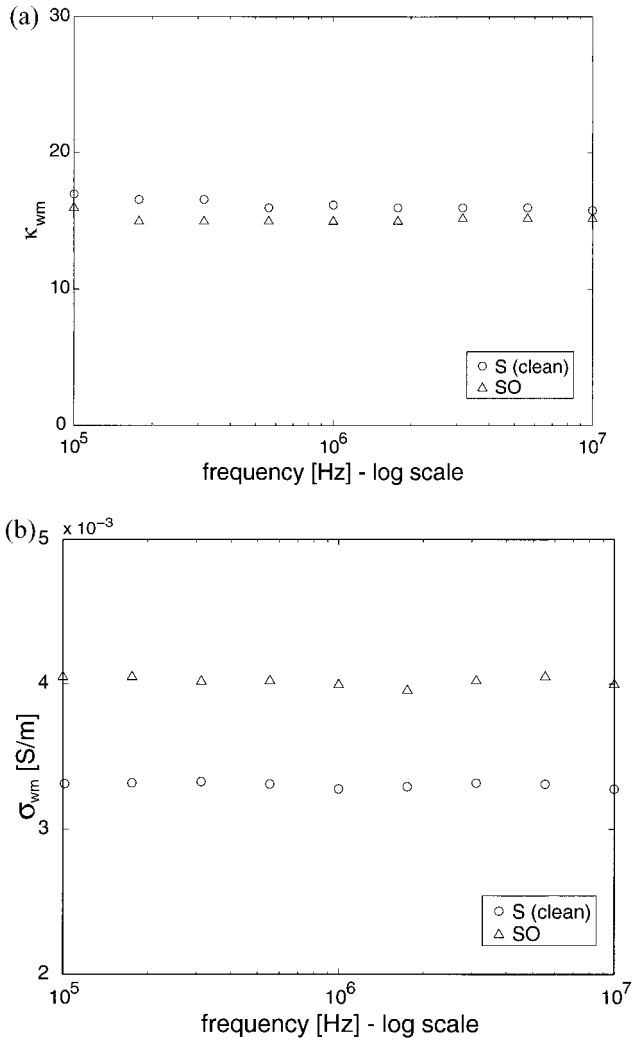

Figure 7. (a) Wetted matrix dielectric constant κ_{wm} and (b) wetted matrix conductivity σ_{wm} for sand samples (1) S (clean) and (2) SO (oil-bearing hydrophobic) over the frequency range 100 kHz to 10 MHz.

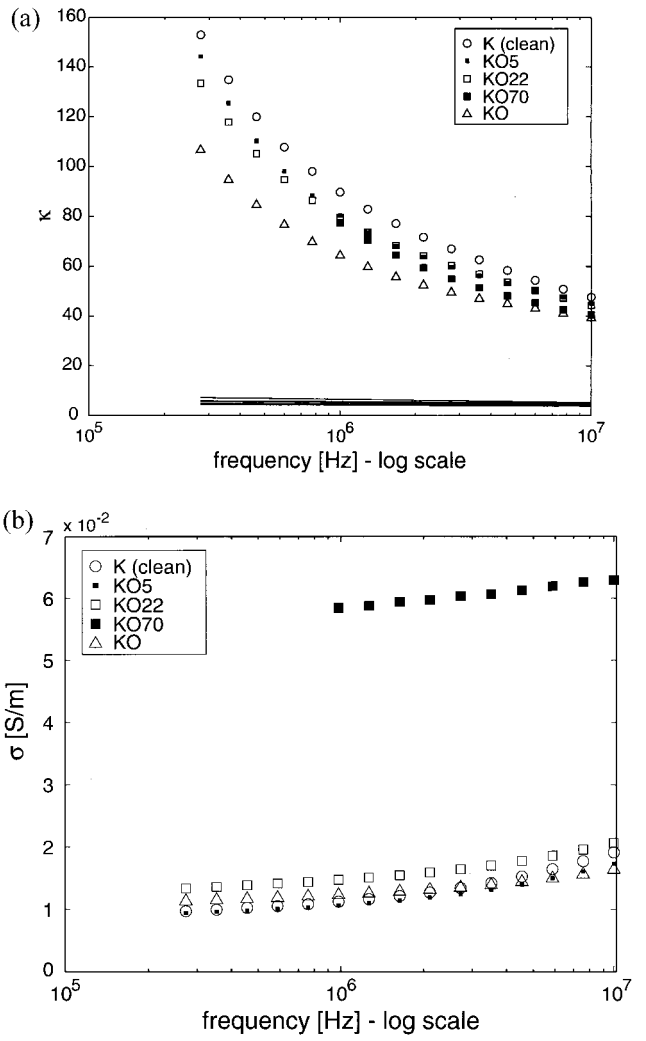

Figure 8. (a) Bulk dielectric constant κ and (b) bulk conductivity σ for kaolinite samples (1) K (clean), (2) KO (oil-bearing hydrophobic), (3) KO5 (5 mg/g oil-bearing), (4) KO22 (22 mg/g oil-bearing), and (5) KO70 (70 mg/g oil-bearing). The solid lines in Figure 8a represent the range for the room-dry bulk κ values. The room-dry bulk σ values are all close to the zero axis on this scale.

the sample to further reduce the water-wetted surface area. In order to quantify this parameter, we calculated a sorbed water index SWI_j

$$\mathrm{SWI}_j = \frac{mw90_j m_j}{mw90_K m_K}, \tag{23}$$

where $mw90$ is the amount of water present at 90% relative humidity, m is the mass of the solid sample, the subscript j refers to sample j (j = K, KO, KO5, KO22, or KO70), and the subscript K refers to sample K.

We used the sorbed water index to examine the trend in the wetted matrix dielectric constants κ_{wm} of the samples (see Figure 11) up to 4 MHz, which is the frequency defined by similar studies as the cutoff above which errors due to higher-order dynamic effects are introduced [*Knight and Nur*, 1987; *Knight and Abad*, 1995]. Note that although the data points for each sample have the same value of SWI, they have been offset horizontally in order to allow differentiation of the error bars, which would otherwise overlap. The plot reveals a general decline in the value of κ_{wm} as the solid surface becomes more hydrophobic (or less water wetted). The trend is clear for the two lowest frequencies (that is, the two top lines in Figure 11, which correspond to 1 MHz and 1.4 MHz), but the results between 1.4 MHz and 4 MHz are complicated by the crossover of κ_{wm} responses previously discussed. However, the limits of experimental uncertainty as defined by the error bars do not rule out the possibility that a consistent, proportional trend exists between κ_{wm} and SWI.

As a simple, physical explanation for our results, we return to the idea that the wetted matrix parameters reflect the dielectric response of the interfacial region of solid, brine, and, if present, oil. As the amount of oil sorbed onto the surface increases, the amount of water-wetted solid surface decreases, thus limiting the formation of a surface water layer. The role of surface water has been investigated in numerous studies, and its tendency to increase the measured dielectric constant is often interpreted in terms of the rotational or orientational polarization of the bound layer as well as conductivity heterogeneities in the system [*McCafferty et al*., 1970; *Knight and Nur*, 1987; *Glover et al*., 1994; *Chelidze et al*., 1999]. Orientational

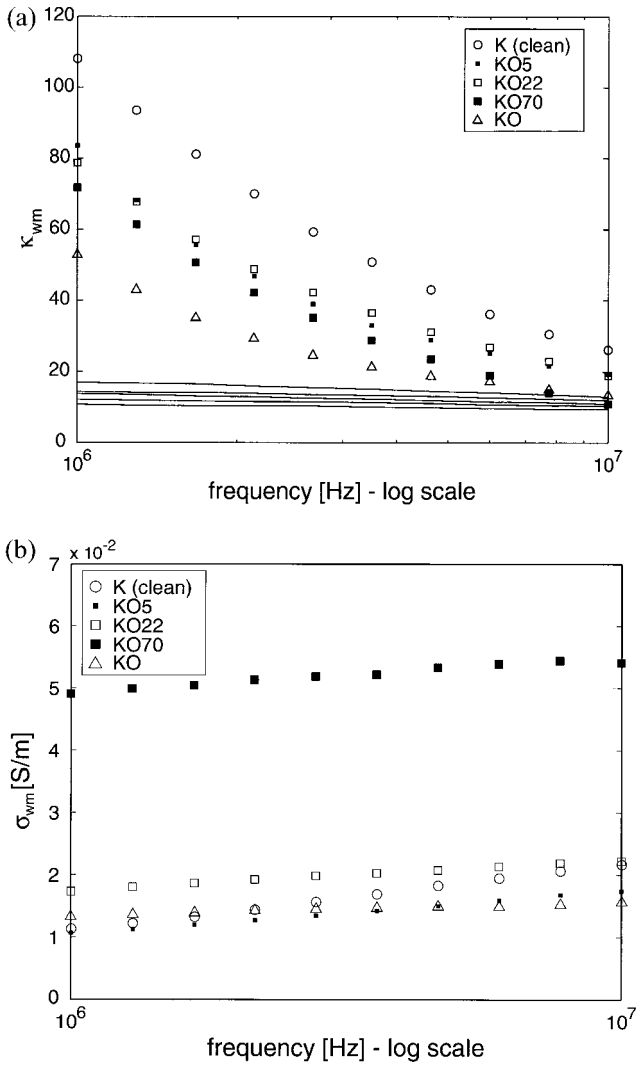

Figure 9. (a) Wetted matrix dielectric constant κ_{wm} and (b) wetted matrix conductivity σ_{wm} for kaolinite samples (1) K (clean), (2) KO (oil-bearing hydrophobic), (3) KO5 (5 mg/g oil-bearing), (4) KO22 (22 mg/g oil-bearing), and (5) KO70 (70 mg/g oil-bearing) over the frequency range 1 MHz to 10 MHz. The solid lines in Figure 9a represent the range for the room-dry matrix κ values. The room-dry matrix σ values are all close to the zero axis on this scale.

polarization is present as a "fast" relaxation mechanism in most water-bearing rocks and, as a general rule, is responsible for κ increases of the order of 10–50 in the 10–100 kHz range [*Chelidze et al*., 1999]. It is possible that we are observing some effect of orientational polarization in our experiments conducted in the low megahertz range; however, there is another mechanism which we must consider. In the presence of a surface water layer, tangential displacements of charges within the layer can result in "film polarization," a mechanism which essentially produces a multitude of grain-sized capacitors, thereby enhancing the dielectric response of the system. This interpretation was used by *Knight and Nur* [1987] to explain the rapid increase in κ of sandstones (60 kHz to 1.2 MHz) upon introduction of the first 2 nm of water to the internal surfaces of the pore space. Along with the space-charge polarization of diffuse ions, film polarization can also account for anomalously large values of κ at low frequencies [*Wong*, 1979; *Chelidze et al*.,

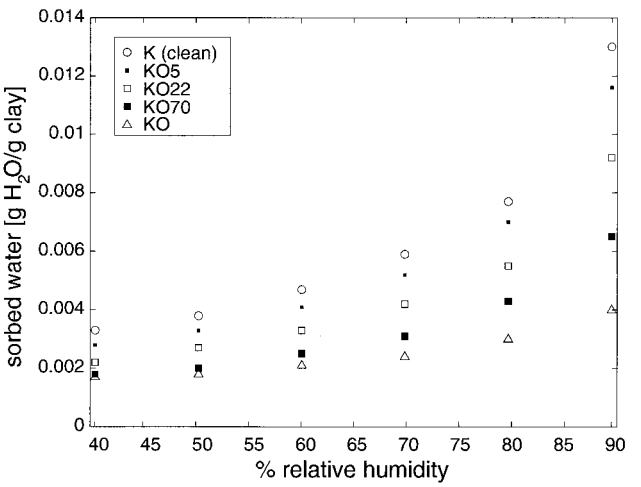

Figure 10. The amount of water in grams sorbed onto the surface of a gram of clay as a function of relative humidity for kaolinite samples (1) K (clean), (2) KO5 (5 mg/g oil-bearing), (3) KO22 (22 mg/g oil-bearing), (4) KO70 (70 mg/g), and (5) KO (oil-bearing hydrophobic).

1999]. In effect then, the sorption of oil onto the solid surface interferes with the formation of a surface water layer, and the observed effect is a decrease in the dielectric constant of the rock/brine system as it loses its ability to polarize through certain surface-related mechanisms.

With between 5 and 70 mg of oil per gram of clay, we have simulated levels of contamination similar to prepared laboratory samples (60–64 mg/g) [*Dorn and Salanitro*, 2000] and real soil samples (50 mg/g) [*Wattiau et al*., 1999] in other crude oil remediation studies. For comparison, typical levels of gasoline spills in soil range from 0.3 to 55 mg/g [*Baker et al*., 2000; *Hayden et al*., 1997], while residual PCE contamination has been measured in quantities from 8 to 44 mg/g [*Bradford et al*., 1999]. While further laboratory studies are needed to fully

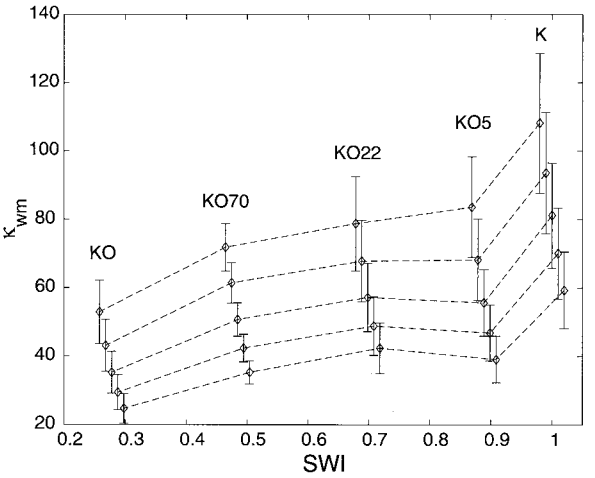

Figure 11. The dependence of wetted matrix dielectric constant κ_{wm} on the amount of water-wetted surface, represented by the sorbed water index SWI, over the frequency range 1 MHz (top line) to 4 MHz (bottom line). Note that although the data points for each sample have the same value of SWI, they have been offset horizontally in order to allow differentiation of the error bars.

understand and quantify the relationship in Figure 11, the observed tendency of κ to decrease with the sorption of crude oil in such amounts suggests that dielectric measurements may provide a means of detecting sorbed contaminants. This study and previous studies indicate that the sensitivity of dielectric measurements to the presence of sorbed contaminants will be greatest at kilohertz to low megahertz frequencies. In the laboratory such measurements can be made using network or impedance analyzers. In the field, measurements at these frequencies are below the range of typical borehole or surface radar systems but fall within the operating frequency range of the new geophysical systems referred to as very early time electromagnetics [*Wright et al*., 1995].

6. Concluding Remarks

In the case of the silica sand samples, we found little difference between clean and contaminated surfaces with dielectric measurements, presumably because of the very low surface area (0.2 m^2/g) of the interfacial region. However, experiments on kaolinite samples confirmed that the chemical nature of the solid surface can modify solid-water interactions and, consequently, the dielectric behavior of the system as a whole. The analysis presented here indicates that the presence of sorbed oil increases the hydrophobicity of the sample surface, diminishing the strength of solid-water interactions sufficiently in high surface area materials to produce a detectable change in dielectric properties. Although the nonlinearity of the plot in Figure 11 suggests that there is not a simple relationship between dielectric constant and the amount of sorbed oil, the results are, nevertheless, encouraging for the use of field dielectric measurements to detect and monitor contaminants in high surface area materials. Through laboratory experiments and an analysis based on effective medium theory this study has shown that the presence of sorbed contaminants on the solid surface is an important factor in determining the dielectric response of partially saturated geologic materials.

Acknowledgments. The authors wish to thank David Redman, André Revil, and one anonymous reviewer for their constructive comments. This research was supported in full by funding to R. Knight under grant DE-FG07-96ER14711, Environmental Management Science Program, Office of Science and Technology, Office of Environment Management, United States Department of Energy (DOE). However, any opinions, findings, conclusions, or recommendations expressed herein are those of the authors and do not necessarily reflect the views of DOE.

References

Baker, R. J., A. L. Baehr, and M. A. Lahvis, Estimation of hydrocarbon biodegredation rates in gasoline-contaminated sediment from measured respiration rates, *J. Contam. Hydrol*., *41*, 175–192, 2000.

Börner, F., M. Gruhne, and J. Schön, Contamination indications derived from electrical properties in the low frequency range, *Geophys. Prospect*., *41*, 83–98, 1993.

Bradford, S. A., R. A. Vendlinksi, and L. M. Abriola, The entrapment and long-term dissolution of tetrachloroethylene in fractional wettability porous media, *Water Resour. Res*., *35*, 2955–2964, 1999.

Chelidze, T. L., Y. Guéguen, and C. Ruffet, Electrical spectroscopy of porous rocks: A review, II, Experimental results and interpretation, *Geophys. J. Int*., *137*, 16–34, 1999.

Cole, K. S., and R. H. Cole, Dispersion and absorption in dielectrics, I, Alternating current characteristics, *J. Chem. Phys*., *9*, 341–351, 1941.

Debye, P., *Polar Molecules*, Dover, Mineola, N. Y., 1929.

Dorn, P. B., and J. P. Salanitro, Temporal ecological assessment of oil contaminated soils before and after bioremediation, *Chemosphere*, *40*, 419–426, 2000.

Endres, A. L., and R. Knight, A theoretical treatment of the effect of microscopic fluid distribution on the dielectric properties of partially saturated rocks, *Geophys. Prospect*., *40*, 307–324, 1992.

Feng, S., and P. N. Sen, Geometrical model of conductive and dielectric properties of rocks, *J. Appl. Phys*., *58*, 3236–3243, 1985.

Garrouch, A. A., and M. M. Sharma, The influence of clay content, salinity, stress and wettability on the dielectric properties of brine-saturated rocks: 10 Hz to 10 MHz, *Geophysics*, *58*, 909–917, 1990.

Glover, P. W. J., P. G. Meredith, P. R. Sammonds, and S. A. F. Murrel, Ionic surface electrical conductivity in sandstone, *J. Geophys. Res*., *99*, 21,635–21,650, 1994.

Hayden, N. J., T. C. Voice, and R. B. Wallace, Residual gasoline saturation in unsaturated soil with and without organic matter, *J. Contam. Hydrol*., *25*, 271–281, 1997.

Jackson, J. D., *Classical Electrodynamics*, John Wiley, New York, 1975.

Knight, R. J., and A. Abad, Rock/water interaction in dielectric properties: Experiments with hydrophobic sandstones, *Geophysics*, *60*, 431–436, 1995.

Knight, R. J., and A. Endres, A new concept in modeling the dielectric response of sandstones: Defining a wetted rock and bulk water system, *Geophysics*, *55*, 586–594, 1990.

Knight, R. J., and A. Nur, The dielectric constant of sandstones, 60 kHz to 4 MHz, *Geophysics*, *52*, 644–654, 1987.

Lange, J. N., Microwave properties of saturated reservoirs, *Geophysics*, *48*, 367–375, 1983.

Li, C., The effect of surface wettability on the dielectric properties of contaminated sands, M.Sc. thesis, Univ. of British Columbia, Vancouver, British Columbia, Canada, 1999.

McCafferty, E., V. Pravdic, and A. C. Zettlemoier, Dielectric behaviour of adsorbed water films on the 2-Fe_2O_3-surface, *Trans. Faraday Soc*., *66*, 1720–1725, 1970.

Olhoeft, G. R., Geophysical detection of hydrocarbon and organic chemical contamination, in *Proceedings of the Symposium on the Application of Geophysics to Engineering and Environmental Problems* (*SAGEEP*), *Oakbrook, IL*, pp. 587–594, Environ. and Eng. Geophys. Soc., Denver, Colo., 1992.

Raistrick, I. D., C. Ho, and R. A. Huggins, Ionic conductivity in some lithium silicates and aluminosilicates, *J. Electrochem. Soc*., *123*, 1469–1476, 1976.

Santamarina, B. L., and M. Fam, Dielectric permittivity of soils mixed with organic and inorganic fluids (0.02 GHz to 1.3 GHz), *J. Environ. Eng. Geophys*., *2*, 37–51, 1997.

Sen, P. N., C. Scala, and M. H. Cohen, A self-similar model for sedimentary rocks with application to the dielectric constant of fused glass beads, *Geophysics*, *46*, 781–795, 1981.

Shen, L. C., W. C. Savre, J. M. Pierce, and K. Athavale, Dielectric properties of reservoir rocks at ultra-high frequencies, *Geophysics*, *50*, 692–704, 1985.

Stumm, W., *Chemistry of the Solid-Water Interface: Processes at the Mineral-Water and Particle-Water Interface in Natural Systems*, John Wiley, New York, 1992.

Vanhala, H., H. Soininen, and I. Kukkonen, Detecting organic chemical contaminants by spectral-induced polarization method in glacial till environment, *Geophysics*, *57*, 1014–1017, 1992.

Ward, S. H., and G. W. Hohmann, Electromagnetic theory for geophysical applications, in *Electromagnetic Methods in Applied Geophysics*, edited by M. N. Nabighian, pp. 130–311, Soc. of Explor. Geophys., Tulsa, Okla., 1988.

Wattiau, P., D. Springael, J. Gemoets, L. Diels, and G. Cornelis, Bacterial monitoring of a crude oil-contaminated soil undergoing laboratory-scale bioremediation, in *Novel Approaches for Bioremediation of Organic Pollution*, edited by R. Fass, Y. Flashner, and S. Reuveny, pp. 181–188, Kluwer Acad., Norwell, Mass., 1999.

Wharton, R. P., G. A. Hazen, R. N. Rau, and D. L. Best, Electromagnetic propagation logging: Advances in technique and interpretation, *Soc. Petr. Eng., AIME*, *29*, paper 9267, 1980.

Wong, J., An electrochemical model of the induced-polarization phenomenon in disseminated sulfide ores, *Geophysics*, *44*, 1245–1265, 1979.

Wright, D. L., T. P. Grover, V. F. Labson, L. Pellerin, K. J. Ellefsen, and J. A. Bradley, Tomography between wells, a transient dielectric logging tool, and the very early time electromagnetic (VETEM) system, in *Proceedings of the Symposium on the Application of Geophysics to Engineering and Environmental Problems* (*SAGEEP*), *Or-*

lando, Fla., pp. 501–510, Environ. and Eng. Geophys. Soc., Denver, Colo., 1995.

Zbik, M., and R. Smart, Nanomorphology of kaolinites: Comparative SEM and AFM studies, *Clays Clay Miner.*, *46*, 153–160, 1998.

R. Knight, Department of Geophysics, Stanford University, Mitchell Building, Room 360, Stanford, CA 94305. (knight@pangea.stanford.edu)

C. Li, Department of Atmospheric Sciences, University of Washington, Seattle, Washington. (camille@atmos.washington.edu)

P. Tercier, Department of Earth and Ocean Sciences, University of British Columbia, Vancouver, British Columbia, Canada V6T 1Z4. (tercier@geop.ubc.ca)

(Received June 1, 2000; revised December 4, 2000; accepted December 27, 2000.)